Int. J. Heat Mass Transfer. Vol. 36, No. 5, pp. 1333–1345, 1993
Printed in Great Britain

0017-9310/93 $6.00+0.00

Unsteady thermosolutal opposing convection of liquid–water mixture in a square cavity—II. Flow structure and fluctuation analysis

J. CHANG and T. F. LIN
Department of Mechanical Engineering, National Chiao Tung University, Hsinchu, Taiwan, Republic of China

(*Received* 7 *February* 1991 *and in final form* 1 *June* 1992)

Abstract—Effects of buoyancy ratio on the flow structure and fluctuating characteristics of the velocity, temperature and concentration fields are numerically investigated for a liquid–water mixture cavity subject to opposing horizontal thermal and solutal buoyancies at high thermal and solutal Rayleigh numbers. Three different flow structures, namely, the multilayer, mixed and secondary cell flows, were predicted. Time histories and power spectra for flow variables probed at several locations indicate that the flow is highly unstable. The collision of the thermally and solutally driven cells causes the secondary cell flow to be chaotic. Moreover, flow bifurcation is noted.

1. INTRODUCTION

THE OPPOSING thermosolutal convection of a liquid mixture in a cavity is inherently unstable due to the counterrotating recirculating flow driven by the opposing thermal and solutal buoyancies. This unstable flow and the associated heat and mass transfer are known to have deleterious effects on a growing crystal. A thorough understanding of these unstable phenomena is of great importance in improving the processes of crystal growth.

Depending on the buoyancy ratio, various flow patterns were noted in the experiments of Jiang *et al.* [1] in shallow enclosures. In particular, multilayer, secondary cell and mixed flow structures were observed. Significant fluctuations in velocity, temperature and concentration can be observed in the secondary cell flow in which the primary flow driven by the thermal buoyancy along the side walls is deflected away from the walls by the secondary cells driven by the solutal buoyancy in the corners, which in turn induces unsteady solutal boundary layers. The effects of the unsteady solutal boundary layer on the unsteady mass transfer process are directly attributed to the unsteady secondary cell flow generated by the thermosolutal instability. When the blobs resulting from the squeezing of the opposing thermal and solutal boundary layers are broken off from the intrusive layers, the surrounding lighter or heavier fluid tends to rush in to maintain the local solutal equilibrium. These complex processes result in an instant thinning of the solutal boundary layer around the location where the blobs leave and increase the mass transfer rate at the same time. It is believed that the Seiche fluctuating modes are related to the swaying of the solutal boundary layer. Similar investigations were conducted by Lee *et al.* [2, 3] for tall enclosures. The development of the multilayer flow structure was clearly illustrated in their experimental and numerical studies. To assist our understanding on the oscillatory motions in the thermosolutally driven cavity flow, the literature on the oscillations in thermally driven natural convection at high Rayleigh number is briefly reviewed in the following.

Unstable fluid flow and heat transfer in a rectangular cavity with differentially heated vertical side walls received some attention in the last decade. Based on scale analysis and numerical simulation, Patterson and Imberger [4] classified the transient flow regimes according to the relative values of the Rayleigh number, Prandtl number and aspect ratio. The time and length scales for various flow regimes were proposed. They suggested that a cavity-scale internal seiche may be induced by the tilting of the isotherms as the hot and cold intrusion layers discharged from the vertical side wall boundary layers cross the cavity and meanwhile spread to match the primary internal cell. Ivey [5] conducted a set of experiments to test the above hypothesis. Temperature traces clearly showed short-lived and large-amplitude fluctuations. The source of these oscillations was considered to be the results of the internal hydraulic jumps in the cavity. Numerical simulation based on Ivey's experiments carried out by Schladow *et al.* [6] clearly showed the presence of long-period oscillations for $Ra_t = 2 \times 10^9$. Later Schladow [7] also noted the presence of short-period oscillations. The long-period oscillations were shown to be the cavity-scale mode resulting from the tilting of the isotherms. The short-period oscillations were found to be the results of the boundary layer instability. By including the sidewall effects, Patterson and Imberger [4] suggested a relatively simple criterion for the presence of internal wave oscillation for $Pr \geqslant 1$ and $A \leqslant 1$. Moreover, they concluded that

NOMENCLATURE

D solutal diffusivity
g gravitational acceleration
Gr_t, Gr_s Grashof numbers of heat and mass transfer
H height of enclosure
N buoyancy ratio
Nu_x, $\overline{Nu}$ local and average Nusselt numbers
n time step
P, p_d dimensionless and dynamic pressures
Pr, Sc Prandtl and Schmidt numbers
Ra_t, Ra_s thermal and solutal Rayleigh numbers
Sh_x, $\overline{Sh}$ local and average Sherwood numbers
t, τ dimensional and dimensionless time
T^0, T dimensional and dimensionless temperatures
T_H^0, T_C^0 hot and cold wall temperatures
u, v vertical and horizontal velocity components
U, V dimensionless vertical and horizontal velocity components
W_{1i}^0, W dimensional and dimensionless mass fractions of species 1
W_{1H}^0, W_{1L}^0 high and low mass fractions of species 1.

Greek symbols
α thermal diffusivity of the mixture
β_t, β_s thermal and solutal volumetric expansion coefficients
ΔT^0, ΔW_1^0 temperature and concentration differences, $(T_H^0 - T_C^0)$ and $(W_{1H}^0 - W_{1L}^0)$
δ_t, δ_s thermal and solutal boundary layer thickness
Γ concentration ratio
ν kinematic viscosity of the mixture
ρ mass density of the mixture.

the cavity-scale internal wave activity is due to the 'pile-up' of the horizontal intrusions at the far ends. Paolucci and Chenoweth [8] numerically showed the existence of an oscillatory approach to steady-state, oscillatory instabilities, quasi-periodic flow, and chaotic flow for air with a wide range of the Rayleigh number. They found that for aspect ratios of approximately 3 or larger the first transition from steady state is due to instability of the sidewall boundary layers, while for $3 > A \geqslant 1/2$, it is due to internal waves near the departing corners.

The above review clearly indicates that the unsteady oscillatory thermosolutal cavity convection is poorly understood. To delineate the detailed characteristics of the unstable thermosolutal convection in a liquid–water-filled cavity, we continue our numerical simulation to obtain the fluctuating characteristics of the system at high thermal and solutal Rayleigh numbers. Particular attention is devoted to the oscillations associated with various flow patterns for different buoyancy ratios when the system has reached the statistically oscillatory state.

2. FORMULATION AND SOLUTION METHOD

To be investigated is a binary liquid–water mixture at a uniform temperature T_i^0 and concentration W_{1i}^0 contained in a square enclosure with thermally well insulated and impermeable top and bottom walls. At $t \geqslant 0$ decent temperature and concentration differences are imposed across the vertical side walls to produce opposing thermal and solutal buoyancies. The transient fluctuating flow, thermal and solutal characteristics can be predicted, under Boussinesq approximations, by the following nondimensional basic equations:

$$\partial U/\partial X + \partial V/\partial Y = 0 \tag{1}$$

$$\partial U/\partial \tau + U\,\partial U/\partial X + V\,\partial U/\partial Y = -\partial P/\partial X + Pr\,\nabla^2 U + Gr_t \cdot Pr^2 (T + N \cdot W) \tag{2}$$

$$\partial V/\partial \tau + U\,\partial V/\partial X + V\,\partial V/\partial Y = -\partial P/\partial Y + Pr\,\nabla^2 V \tag{3}$$

$$\partial T/\partial \tau + U\,\partial T/\partial X + V\,\partial T/\partial Y = \nabla^2 T \tag{4}$$

$$\partial W/\partial \tau + U\,\partial W/\partial X + V\,\partial W/\partial Y = \nabla^2 W/Le. \tag{5}$$

In writing the above equations the following nondimensional variables were introduced:

$$X = x/H, \quad Y = y/H, \quad U = u/(\alpha/H),$$
$$V = v/(\alpha/H), \quad \tau = \tau/(H^2/\alpha),$$
$$P = p_d/(\rho\alpha^2/H^2), \quad T = (T^0 - T_i^0)/\Delta T^0,$$
$$W = (W_1^0 - W_{1i}^0)/\Delta W_1^0, \quad Pr = \nu/\alpha,$$
$$Sc = \nu/D, \quad Le = Sc/Pr = \alpha/D,$$
$$N = \beta_s \Delta W^0/\beta_t \Delta T^0, \quad Gr_t = g\beta_t H^3 \cdot \Delta T^0/\nu^2,$$
$$Gr_s = g\beta_s H^3 \cdot \Delta W_1^0/\nu^2. \tag{6}$$

The initial conditions are

$$U, V, T, W(X, Y, 0) = 0 \tag{7}$$

and the boundary conditions applied at $t \geqslant 0$ are:

at

$$Y = 0, \quad U = 0, \quad V = \frac{-1}{Le} \cdot \frac{1}{\Gamma} \cdot \frac{\partial W}{\partial X},$$
$$T = T_C = -0.5, \quad W = W_L = -0.5; \tag{8a}$$

at

$$Y = 1, \quad U = 0, \quad V = \frac{-1}{Le} \cdot \frac{1}{\Gamma - 1} \cdot \frac{\partial W}{\partial X},$$

$$T = T_H = 0.5, \quad W = W_H = 0.5; \qquad (8b)$$

at

$$X = 0 \quad \text{and} \quad 1, \quad U = V = \frac{\partial T}{\partial X} = \frac{\partial W}{\partial X} = 0. \qquad (8c)$$

The interface velocities of the binary mixture induced by the mass diffusion at the side walls are specified in equations (8a) and (8b) with $\Gamma = (1 - W^0_{1L})/(W^0_{1H} - W^0_{1L})$.

Five nondimensional governing parameters appear in the above formulation, namely, the Prandtl number Pr, Schmidt number Sc, heat transfer Grashof number Gr_t, buoyancy ratio N, and concentration ratio Γ. The projection method [9] was chosen to numerically solve the time-dependent governing equations in their primitive form with three interlacing staggered grids, respectively, for the horizontal velocity component, vertical velocity component, and scalar variables. This fractional-step method consists of two steps. First, a provisional value is explicitly computed for the velocity field ignoring the pressure gradient. Then, the provisional velocity field is corrected by including the pressure effect and by enforcing the mass conservation at time step $n+1$. Combining these equations yields the pressure Poisson equation. The detailed description of the solution procedures was given in Part I of this investigation [10].

3. RESULTS AND DISCUSSION

Although computations can be performed for any combination of the governing nondimensional parameters, this part is restricted to the exploration of the buoyancy ratio on the flow patterns and the associated fluctuating characteristics for a liquid–water mixture at high thermal and solutal buoyancies. In particular, we fixed Pr, Le, Gr_t and Γ, respectively, at 7.6, 100, 2×10^5 and 50. The criteria for the appearance of various flow patterns were proposed by Jiang *et al.* [1] for shallow enclosures. They gave two critical buoyancy ratios

$$N_c = 0.13 Gr_s^{1/4} A^{-1/2} \qquad (9a)$$

and

$$N_s = 0.39 Gr_s^{1/4} A^{-1/2}. \qquad (9b)$$

For $N \geqslant N_s$, multilayer structure prevails, while secondary cell flow appears for $N \leqslant N_c$. In between for $N_c < N < N_s$, mixed flow results. The above criteria, however, are not directly applicable to the square cavity considered here. In our numerical simulation many different values of the buoyancy ratio were tested to ascertain the boundaries of the flow patterns. These numerical tests indicated that over the range of N from -2 to -5 various flow regimes were observed. It is important to point out that in this study the mass transfer Rayleigh number ($= |N| \cdot Gr_t \cdot Pr \cdot Le$) is in the range 3.04×10^8–7.6×10^8. This high solutal Rayleigh number is expected to induce unstable flow in the cavity due to the solutal buoyancy alone.

3.1. *Multilayer flow*

Multilayer flow structure is normally observed when the buoyancy ratio is above 3.5. Results for a typical case with $N = -5$ are shown in Fig. 1. The flow formation processes of this particular flow pattern after the imposition of the horizontal temperature and concentration gradients are similar to those presented in Part I [10] for $Le = 100$, $N = -5$ and $Gr_t = 10^5$. Basically, for $\tau \leqslant 0.50$ the flow is characterized by a thermally driven clockwise rotating cell in the core region and two solutally driven counterclockwise circulations along the cavity walls. Later, a number of weakly recirculating cells are induced near the horizontal sides by the viscous shearing of the solutally driven cells (Fig. 1(c)). These weakly recirculating cells merge at a later time to form strong cells, as evident from the streamfunction values in Fig. 1(d). These newly formed cells rotate clockwisely as the thermal cell and are stronger than the cells directly driven by the solutal buoyancy.

The counterrotating flow produced by the high thermal and solutal buoyancies is expected to be unstable. This is investigated by examining the time history of an x-component velocity at a certain location over a certain time interval. A periodic variation in U is distinctly noted in Fig. 2. A periodic change in flow pattern is also shown in the figure over a complete period. The merger and breakup of the strong cells adjacent to the top and bottom plates are clearly seen. It is important to note that the period of the velocity oscillation is about 0.015. This period is comparable to the time scale of the solutal boundary layer, $t_s \sim \delta_s^2/D$, or in dimensionless form $\tau_s \sim (\delta_s^2/H^2) \cdot Le$. From the iso-concentration lines in Fig. 1, $\delta_s/H \sim 0.012$ and $\tau_s \sim 0.0144$.

For clear illustration of the multilayer flow structure, Fig. 3 displays the flow pattern shown in Fig. 1(d) and the associate horizontal velocity profile at the vertical midplane. Apparently, five layers can be identified, namely three strong top, middle and bottom layers and two weak intermediate layers. It is important to note that the top and bottom layers which are indirectly induced by the solutal buoyancy circulate clockwisely defying the intuitive sense of the solutal cell circulation. This unusual circulation may be considered as relatively strange if the flow evolution is not carefully traced. This layered structure is in qualitative resemblance with the experimental observation of Jiang *et al.* [1].

3.2. *Secondary cell flow*

When the buoyancy ratio is decreased below -2.1, a single core flow combined with two secondary cells near the vertical walls appears. In such a situation, because the solutal buoyancy is no longer much larger

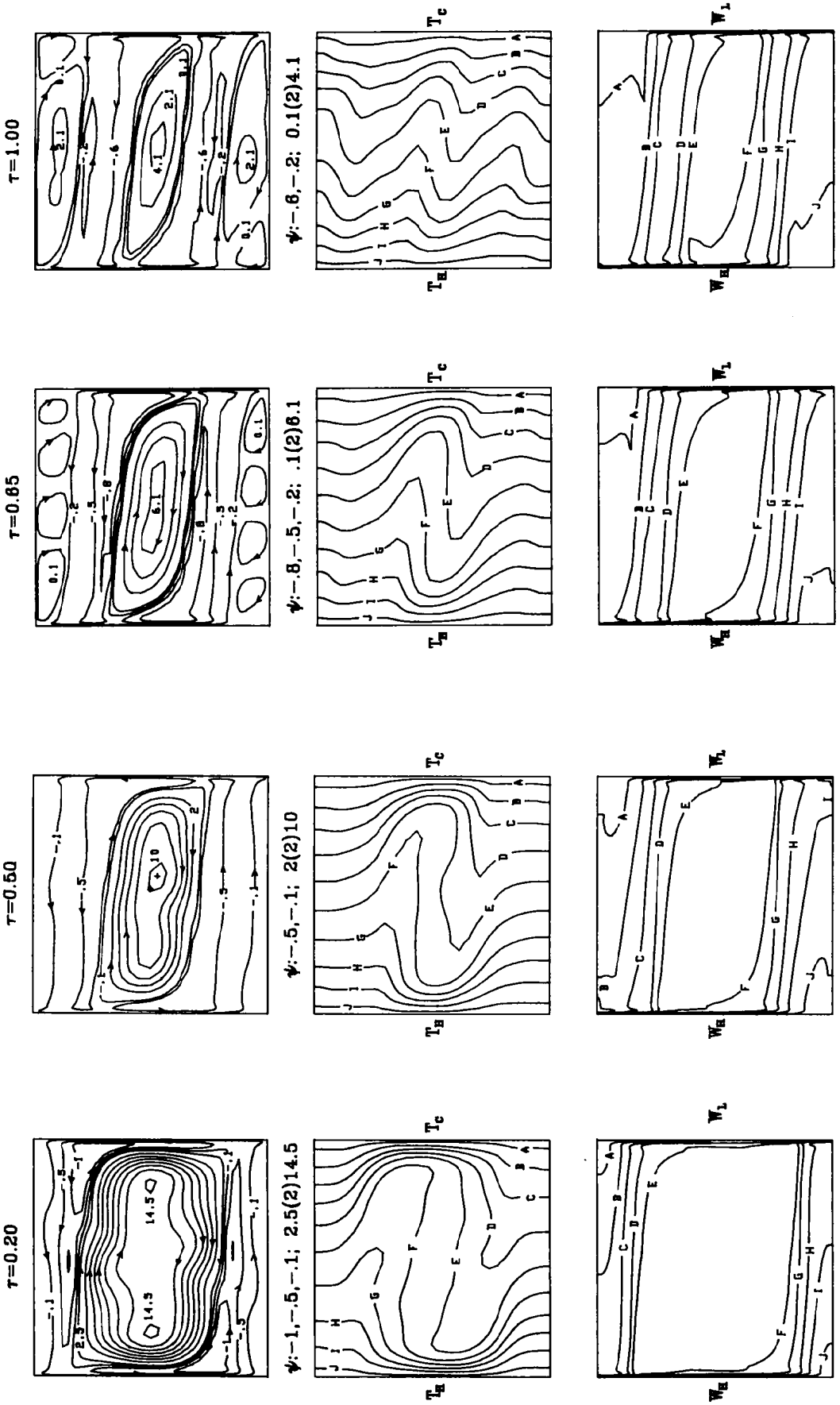

FIG. 1. Time evolution of streamlines, isotherms and iso-concentration lines for $Pr = 7.6$, $Le = 100$, $Gr_t = 2 \times 10^5$, $N = -5$, $\Gamma = 50$ at (a) $\tau = 0.2$, (b) $\tau = 0.5$, (c) $\tau = 0.65$, (d) $\tau = 1.0$. The isotherms and iso-concentration lines are marked in alphabetical order from -0.45 to 0.45 in a constant interval of 0.1.

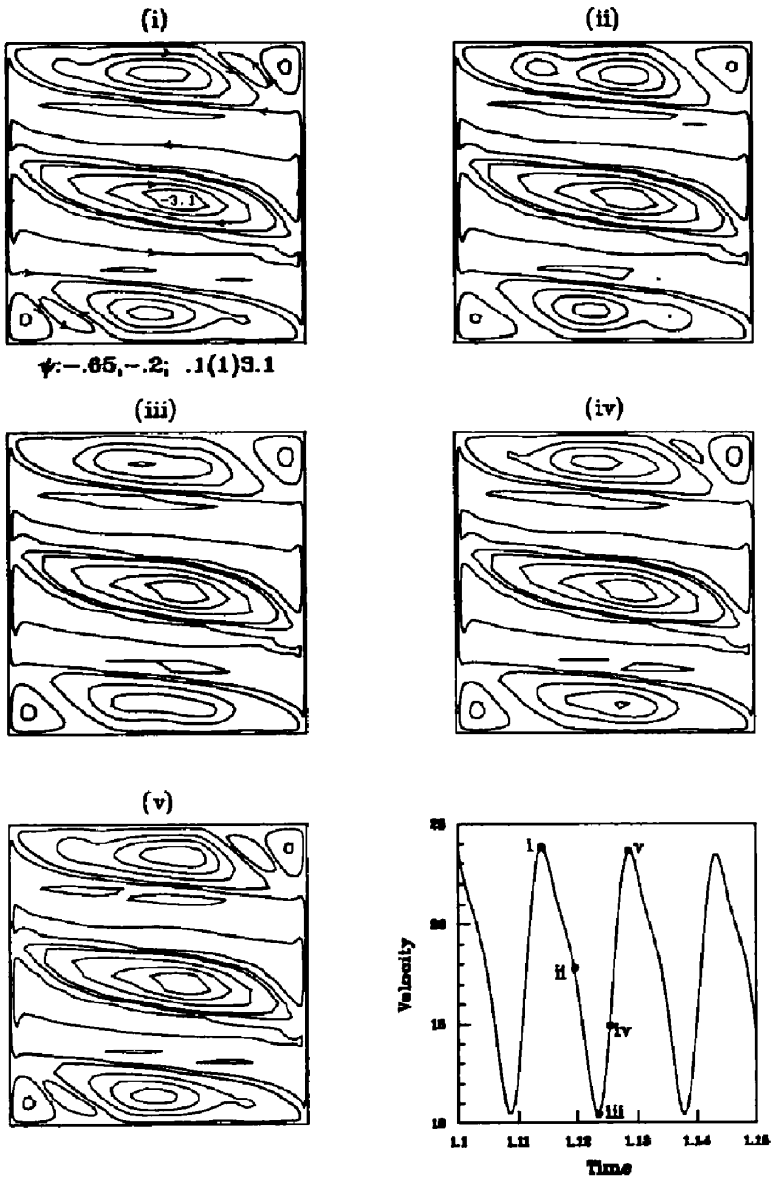

FIG. 2. Streamlines and time history of velocity component U for $Pr = 7.6$, $Le = 100$, $Gr_t = 2 \times 10^5$, $N = -5$, $\Gamma = 50$ at $(X, Y) = (0.0315, 0.9685)$.

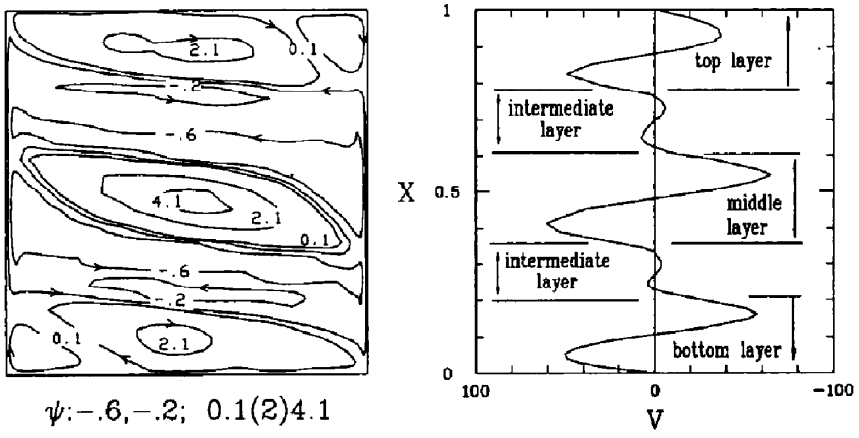

FIG. 3. Detail of the multilayer flow structure for $Pr = 7.6$, $Le = 100$, $Gr_t = 2 \times 10^5$, $N = -5$, $\Gamma = 50$: (a) the flow pattern at $\tau = 1.0$ and (b) the horizontal velocity profile at the vertical midplane.

than the thermal buoyancy, the main flow in the core region is driven by the thermal convection. Figures 4 and 5 show snapshots of the flow at two time instants for $N = -2.1$ and $N = -2$. Upon decreasing the buoyancy ratio to such a level, the solutal buoyancy cannot overcome the opposing thermal buoyancy but yields to the thermal convection. The unicell core flow in Fig. 4, the so-called main stream, is driven by the thermal convection due to the fact that the thermal buoyancy overwhelms the solutal one; and the two solutally driven secondary cells were always found at the departing corners of the thermal boundary layers. Closely inspecting the flow near the vertical walls reveals that two boundary layer flows are separated by a stagnation line [1], so a bidirection flow results in this stagnation region. Focusing on the flow near the right wall, we note that the opposing thermal and solutal buoyancies meet at a neutral balance point somewhere near the wall and the reversed solutally driven flow is stopped at the stagnation line. The stopped flow is then dragged down by the outside core flow, therefore forming a recirculating cell. The net opposing buoyancy forces at this line must be balanced with the viscous shear force induced by the thermal convection in the far field. Since the forces at the stagnation line are neutrally balanced, the position of the line is not predictable. The instability at this line can be interpreted as the result of the thermosolutal instability. Two bidirectional flow streams meet at the stagnation line causing the pressure increase in the vicinity. The lighter fluid is therefore transported horizontally out of the inner wall layer. Later, the horizontal intrusion layer of the lighter fluid is dragged downwards by the core flow. Finally, a plume-like intrusive lighter fluid layer (marked by E) appears in the concentration contours (Fig. 4(a)). The plume will

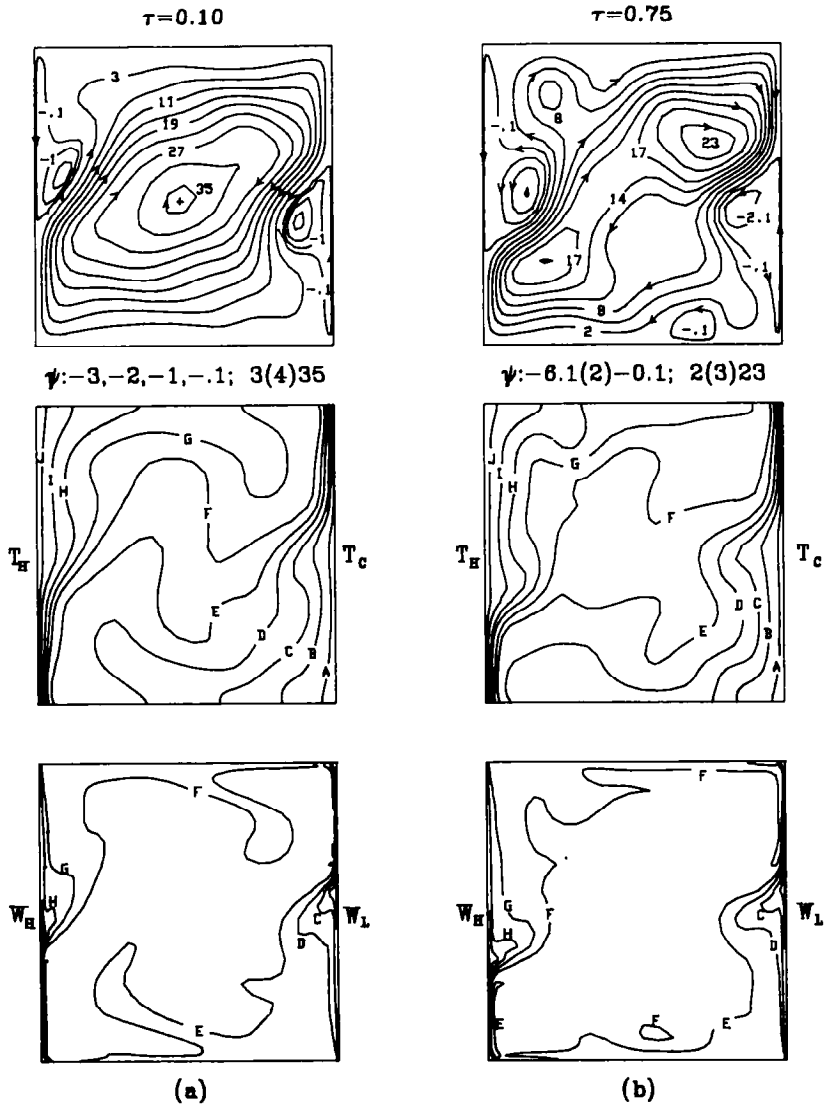

FIG. 4. Time evolution of streamlines, isotherms and iso-concentration lines for $Pr = 7.6$, $Le = 100$, $Gr_t = 2 \times 10^5$, $N = -2.1$, $\Gamma = 50$ at (a) $\tau = 0.1$ and (b) $\tau = 0.75$.

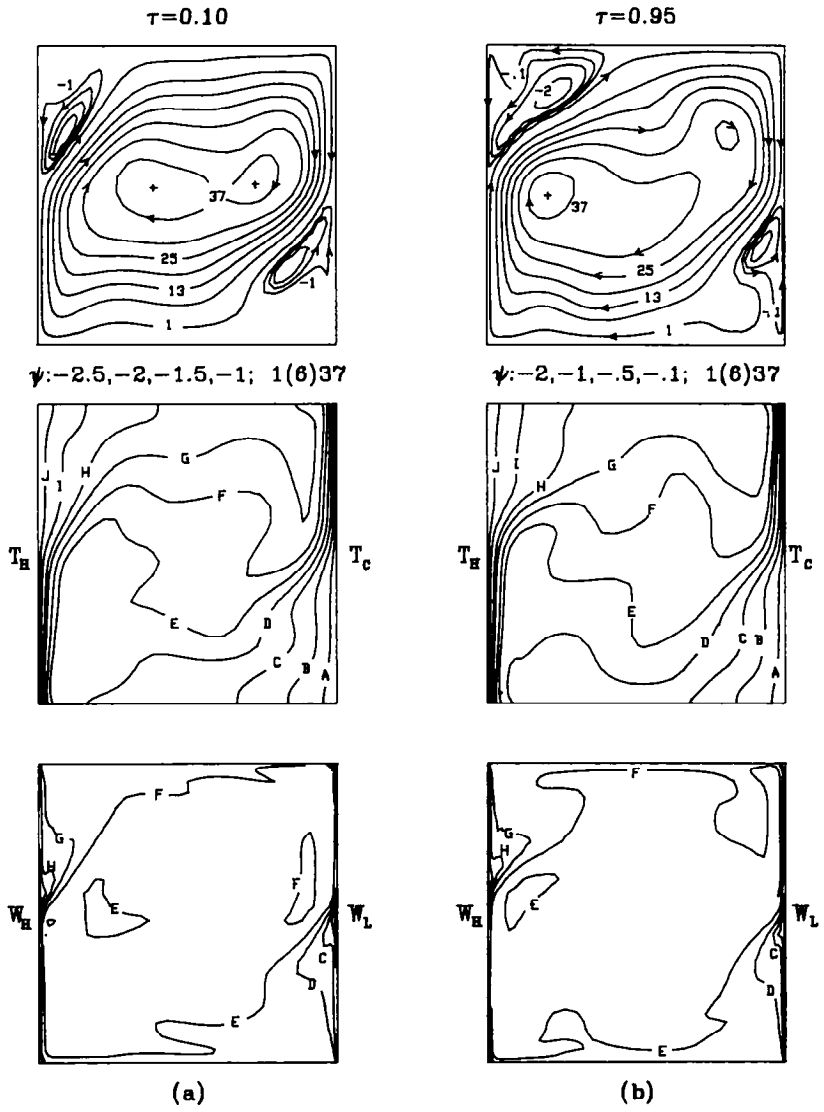

FIG. 5. Time evolution of streamlines, isotherms and iso-concentration lines for $Pr = 7.6$, $Le = 100$, $Gr_t = 2 \times 10^5$, $N = -2$, $\Gamma = 50$ at (a) $\tau = 0.1$ and (b) $\tau = 0.95$.

eventually break off producing blobs, as clearly shown in Figs. 4(b) and 5(a). Owing to the breaking off of those blobs, the lighter blobs leave their original place and the place is refilled by the next coming plume. During these breaking processes, the pressure near the place changes abruptly resulting unstable pressure wave and the internal wave activity in the enclosure is generated. The entire process of the horizontal intrusive fluid layer generation, the subsequent plume entrainment and the breaking off of the blobs may repeat. The particular flow pattern of the main thermal core flow with two solutal cells in the corners results in the boundary layer behavior along the lower half of the left wall and the upper half of the right wall. The weak secondary flow caused only some solutal intrusion along the horizontal walls. Unlike the multilayer flow regime, here the concentration field is not stratified.

3.3. *Mixed flow*

At some intermediate buoyancy ratio with $N = -2.15$, the cavity flow consists of top and bottom fluid layers and two secondary cells along with the thermally driven core flow, as evident from Fig. 6. This particular flow pattern is termed as the mixed flow since it possesses the characteristics of the multilayer flow and the secondary cell flow just discussed. Figure 6(a) clearly shows that a small τ secondary cell flow prevails. The solutal buoyancy is now large enough to drive the flow downwards near the left wall and upwards near the right wall and protrudes towards the opposite walls. Under the counteraction of the core flow the solutally driven cells break up and an interesting flow pattern shown in Fig. 6(b) results. Raising the buoyancy ratio slightly to -2.2, we note in Fig. 7(b) that a big solutal cell extends over the left, top and right walls along with a small solutal cell

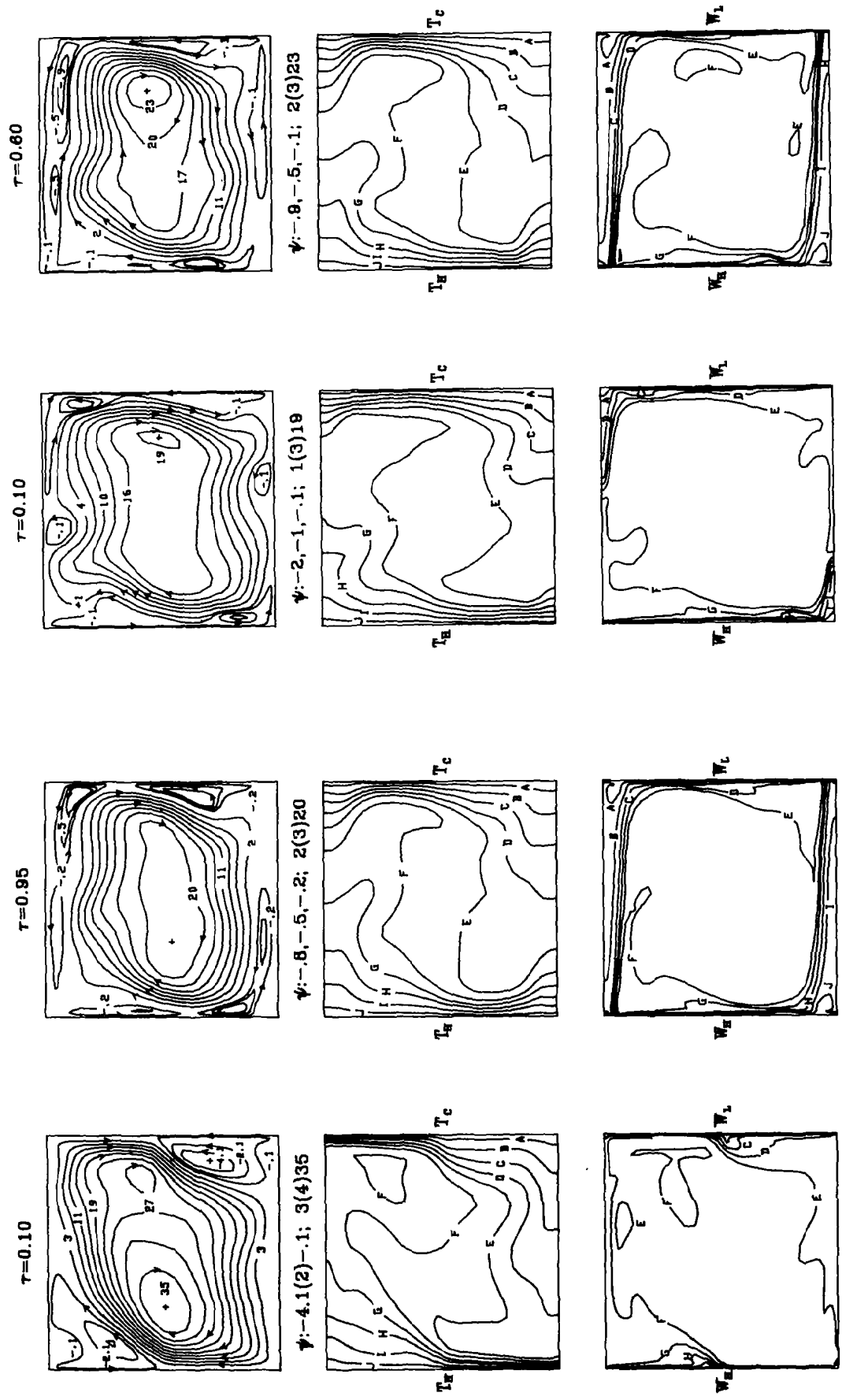

FIG. 6. Time evolution of streamlines, isotherms and iso-concentration lines for $Pr = 7.6$, $Le = 100$, $Gr_t = 2 \times 10^5$, $N = -2.15$, $\Gamma = 50$ at (a) $\tau = 0.1$ and (b) $\tau = 0.95$.

FIG. 7. Time evolution of streamlines, isotherms and iso-concentration lines for $Pr = 7.6$, $Le = 100$, $Gr_t = 2 \times 10^5$, $N = -2.2$, $\Gamma = 50$ at (a) $\tau = 0.1$ and (b) $\tau = 0.6$.

above the bottom wall. We also note some tertiary cells inside the big solutal cell. When the solutal buoyancy is further strengthened by elevating N to -2.5, a bigger solutal cell circulating around all cavity walls finally results (Fig. 8). Inspecting the iso-concentration contours in Figs. 6–8 reveals that the solutal stratification occurs near the top and bottom walls and some blobs appear in the core region. Besides, an increase in the buoyancy ratio causes thicker top and bottom layers.

To get a closer look at the complex flow structures just discussed, in Fig. 9 we plot the vector velocity field, streamlines, isotherms and iso-concentration lines for the right half of the enclosure for various N at large τ. Figure 9(a) indicates that in multilayer structure the core flow driven by the thermal buoyancy and the top and bottom layers driven by the solutal buoyancy move at comparable speeds. Note that two buffer zones (the intermediate layers discussed in Section 3.1) which are relatively stagnant exist between the core flow and the top and bottom layers. Solutal stratification mainly exists in these buffer zones. It is of interest to point out that the isotherms distort in accordance with the direction of the recirculating flow. For the mixed flow regime the thermal core flow dominates over the solutal cells (Figs. 9(b) and (c)). This is also the situation for the secondary cell flow regime shown in Fig. 9(d).

3.4. *Time series and frequency spectra*

To illustrate the fluctuating characteristics of the thermosolutal cavity convection for the various flow structures discussed above, a statistical analysis is required. For a long-time simulation of these flow structures after the initial transients in the time evolution, the time series and spectral analysis of the various flow quantities are presented here. Different dynamic regimes of the flow can be distinguished by

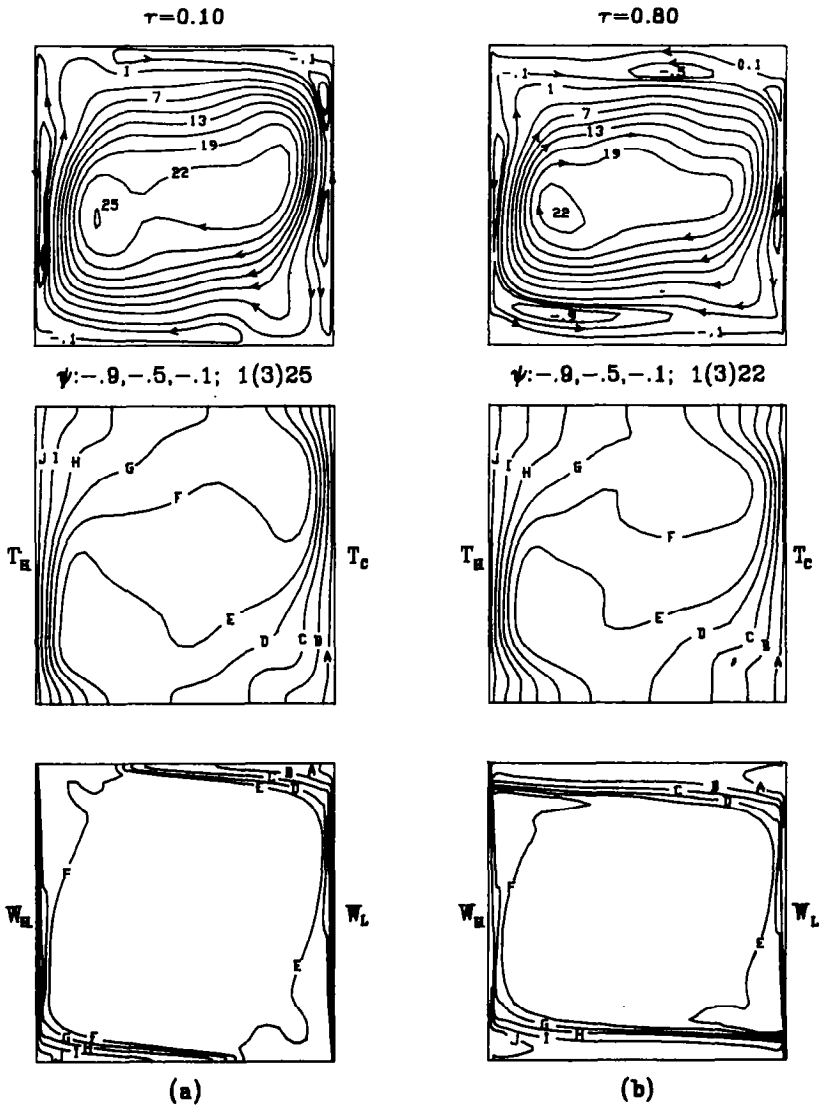

FIG. 8. Time evolution of streamlines, isotherms and iso-concentration lines for $Pr = 7.6$, $Le = 100$, $Gr_t = 2 \times 10^5$, $N = -2.5$, $\Gamma = 50$ at (a) $\tau = 0.1$ and (b) $\tau = 0.8$.

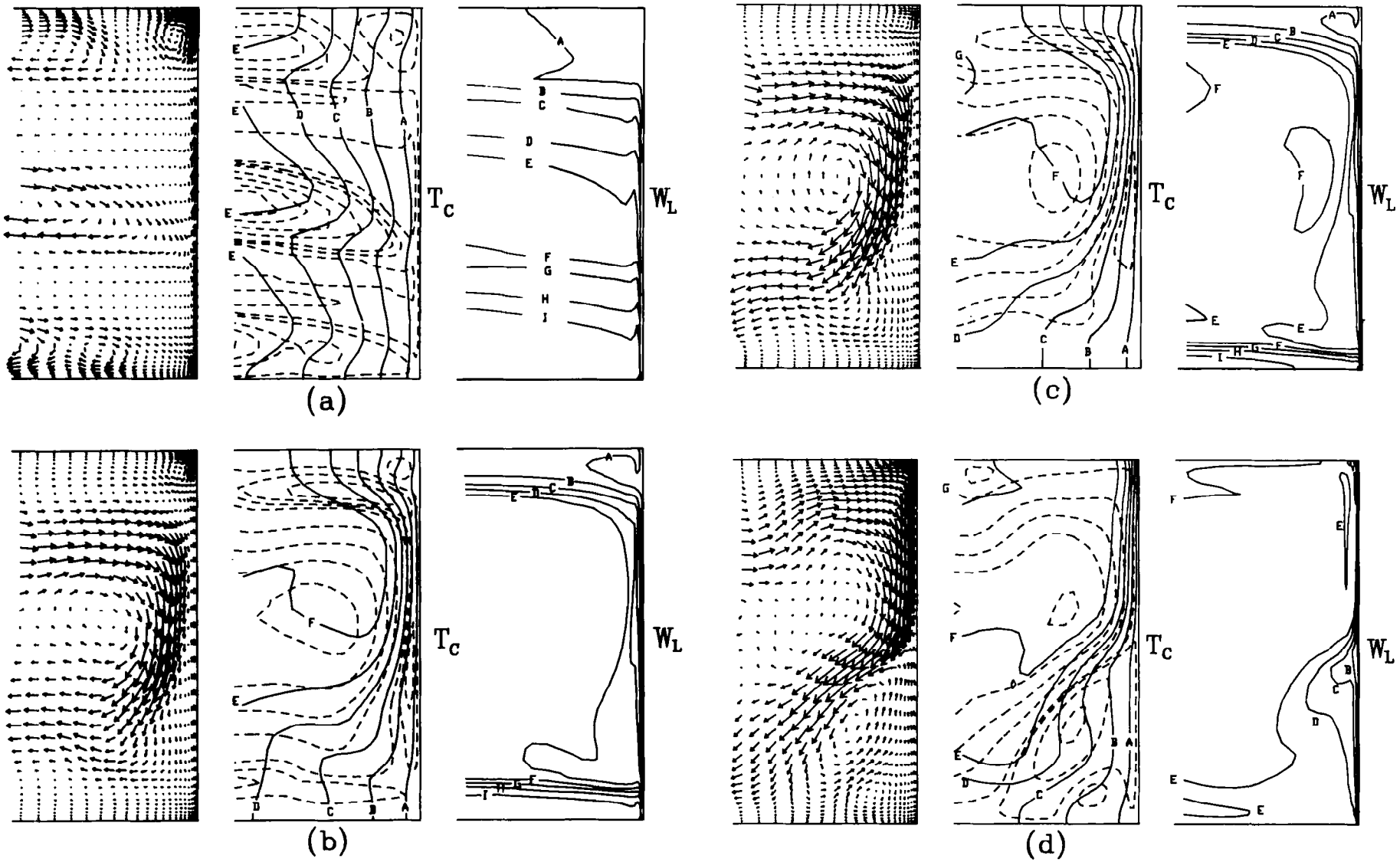

FIG. 9. Zoomed vector velocity field, streamlines (dashed lines), isotherms and iso-concentration lines for $Pr = 7.6$, $Le = 100$, $Gr_t = 2 \times 10^5$, $\Gamma = 50$ at selected time instants: (a) $N = -5$, $\tau = 1.0$; (b) $N = -2.5$, $\tau = 1.0$; (c) $N = -2.2$, $\tau = 0.6$; (d) $N = -2$, $\tau = 0.5$.

examining the high-resolution power spectra of the time records at fixed locations. Power spectra are computed from the square modulus of the fast Fourier transform of U, V, T and W using standard discrete techniques and processed with a Hann window [11]. Results from such spectral analysis along with the time samples for various buoyancy ratios are selectively shown in Figs. 10 and 11 probed at a location at the mid-height of the cavity and within the solutal boundary layer near the hot wall. In multi-layer flow with $N = -5$ the time records show random variation. However, at a lower buoyancy ratio in the mixed flow ($N = -2.5$, -2.2 and -2.15), the signals exhibit some orderness. Particularly at $N = -2.15$, periodic variations are noted for all the detected variables with a high frequency mode enveloped by a low frequency mode. At an even lower buoyancy ratio in the secondary cell flow ($N = -2.1$ and -2), it is surprising to find that the oscillations are rather irregular. This highly unstable secondary cell flow is conjectured to be associated with the collision of thermally driven flow and solutally driven flow at the stagnation line and the release of blobs, as already mentioned above. Inspecting the amplitudes of the fluctuations discloses that the oscillations in U, V, T and W are much more intensive in the secondary cell flow than in the mixed flow. The multilayer flow shows relatively small oscillations in magnitude. The intensity of the fluctuation may vary from one to seven orders when the flow changes from one regime to another. For a given flow structure it is noted that the amplitudes of the temperature and concentration oscillations are much smaller than those of velocity. The above results for the fluctuating characteristics of the

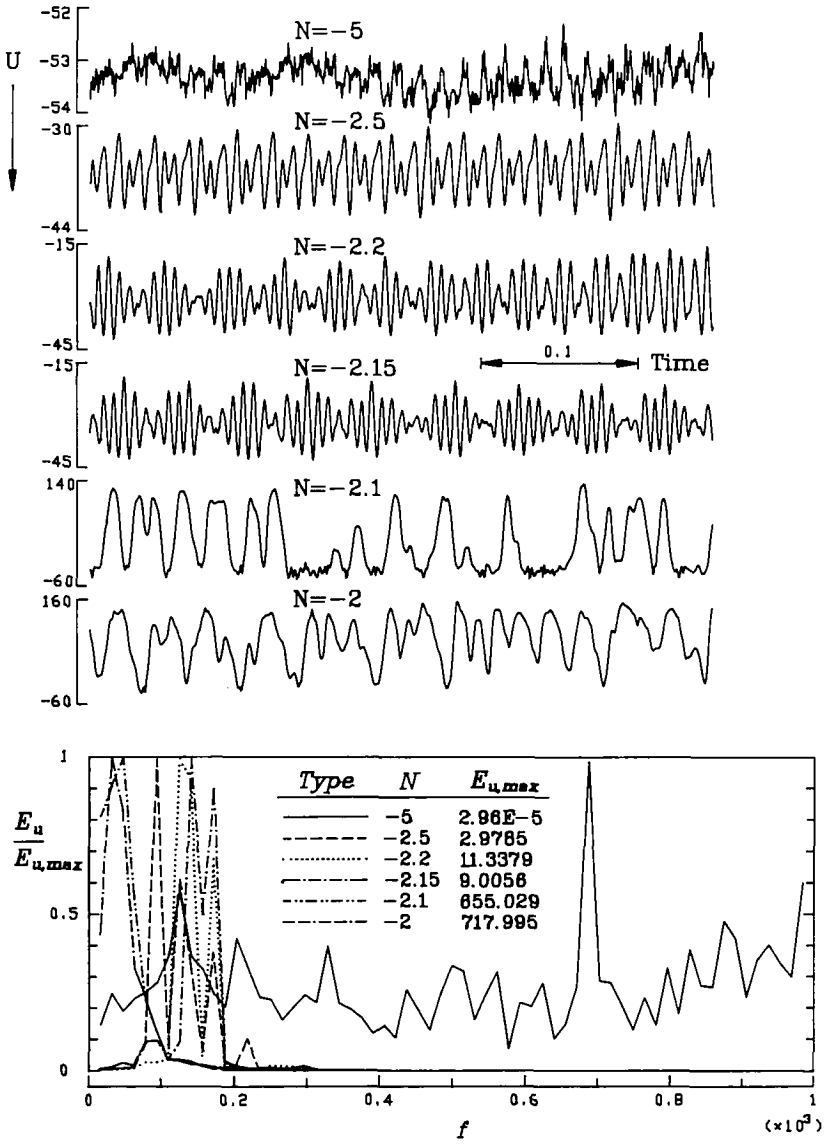

FIG. 10. Time series and normalized power spectra of velocity component U at location $(X, Y) = (0.4729, 0.9944)$ for different buoyancy ratios.

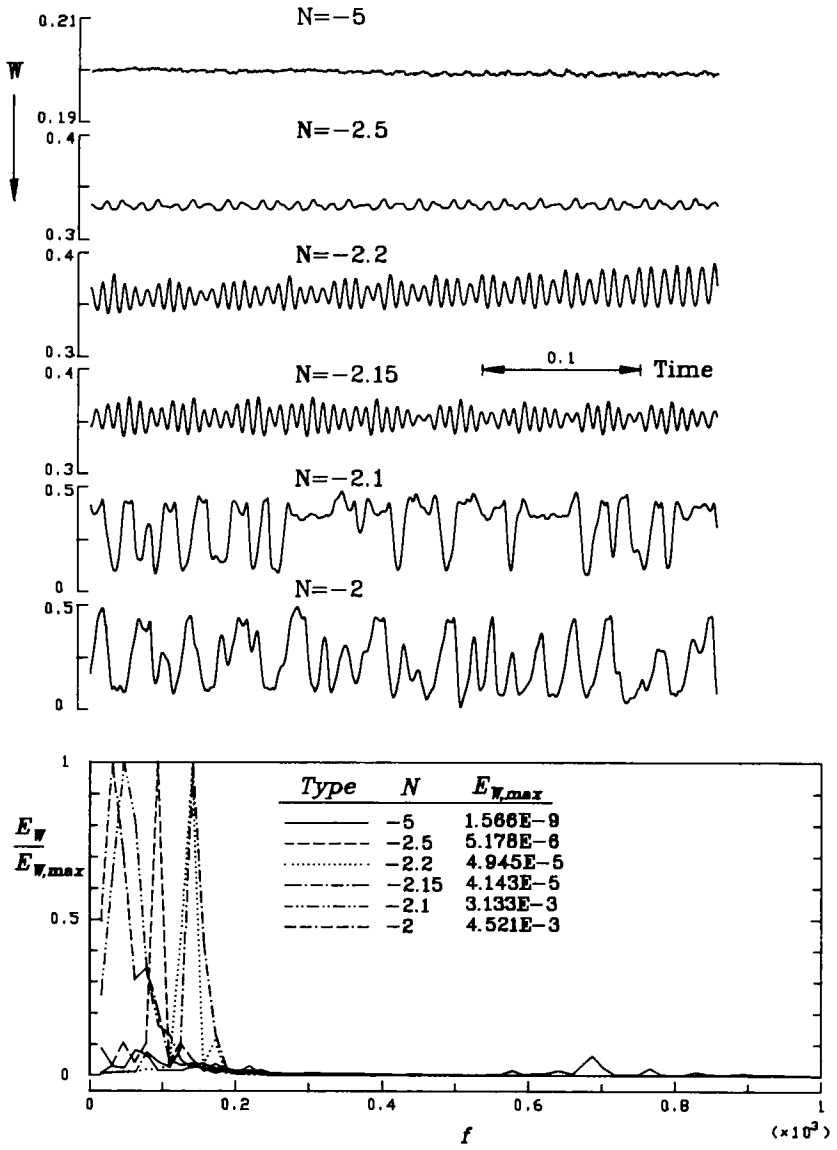

FIG. 11. Time series and normalized power spectra of concentration W at location $(X, Y) = (0.4729, 0.9944)$ for different buoyancy ratios.

time records are in qualitative agreement with the experimental record data of Jiang *et al.* [1].

Results for the power spectra indicate that more than one peak appear for all variables detected for all buoyancy ratios. Particularly for $N = -5$, many peaks exist covering wide ranges of the frequency domain with the fundamental mode at $f = 687.5$. The appearance of several banded peaks in the power spectra reflects the random and irregular nature of the flow [8]. In the mixed flow and secondary cell flow the fundamental frequencies are lower. But in these flow regimes there is no simple trend in the variation of the fundamental frequency with the buoyancy ratio.

As pointed out by Paolucci and Chenoweth [8], the power spectra for the variables probed at different locations may be very different. This is examined by presenting the fundamental frequencies for the time series detected at a point very close to the middle of the bottom plate. It is noted that the fundamental frequency is lowest in the multilayer flow at this new detection point, while the mixed flow has the highest fundamental frequency.

The complex time series and power spectra just discussed are the consequence of the simultaneous presence of the side-wall boundary layer instability, internal wave instability and thermosolutal instability in the flow at high thermal and solutal Rayleigh numbers. The existence of a number of peaks in the power spectra may result from the intricate interactions between these instabilities. At a given N, which modes of instability dominate is still poorly understood. It is beyond our current capability to predict various oscillation modes under different flow conditions.

To further illustrate the temporal evolution of the

unstable transitional flow phenomena in the thermosolutal cavity convection, the phase space trajectories of the temperature and concentration versus velocity component U at a corner point are examined for various buoyancy ratios. The results distinctly show the transition from the nearly periodic fluctuations in the multilayer flow ($N = -5$) to the chaotic variations in the secondary cell flow ($N = -2$) [8].

In the unstable thermosolutal cavity convection it is suggested by Jiang *et al.* [1] that the flow evolution is relatively sensitive to the initial condition. Very different flow patterns may result under different initial conditions. This flow bifurcation phenomenon is investigated by comparing the long-time solutions for $N = -2$ with two different initial flow conditions. When the initial flow is stationary and at uniform temperature and concentration, a secondary cell flow pattern is predicted in Fig. 5. Next, we use the mixed flow structure shown in Fig. 8(a) for $N = -2.5$ as an initial condition and meanwhile reduce the buoyancy ratio from -2.5 to -2 before starting the numerical simulation. The resulting flow and the associated heat and mass transfer characteristics are very different from the secondary cell flow presented in Fig. 5. In fact, it is essentially a mixed flow. In addition to the flow structure, we also examined the time records of U, V and T. The fundamental frequencies, F_s and F_b, are 109.4 and 171.9, respectively, for the simulation with N reducing from -2.5 to -2, in contrast to 46.9 and 140.6 when the initial flow is still.

4. CONCLUDING REMARKS

Through a detailed numerical simulation, three different flow structures were predicted in thermosolutal cavity convection under opposing thermal and solutal buoyancies. At a high buoyancy ratio a multilayer flow prevails, while secondary cell flow dominates at a low buoyancy ratio. In between there is a mixed flow regime. Time-series and power spectra analysis along with the phase space trajectories for U, V, T and W probed at several locations indicate that the multilayer flow is nearly periodic and the secondary cell flow is chaotic. The highly unstable and transitional flow results from the complex interactions between the side-wall boundary layer instability, internal wave instability and thermosolutal instability.

The fluctuating characteristics of the thermosolutal cavity convection show that it is much more complicated than pure thermal convection [8]. To delineate the unstable and transitional thermosolutal convective flow, a thorough understanding of the interactions between various instability mechanisms is needed. Besides, it is recognized that the unstable and transitional flow is essentially three-dimensional, as suggested by Jiang *et al.* [1]. Thus, an extension of the present simulation to three dimensional flow is necessary.

Acknowledgement—The support of this study by the engineering division of National Science Council of Taiwan, R.O.C. through the contract NSC-77-0401-E009-10 is gratefully acknowledged.

REFERENCES

1. H. D. Jiang, S. Ostrach and Y. Kamotani, Thermosolutal convection with opposed buoyancy forces in shallow enclosures, *ASME-HTD* **99,** 53–66 (1988).
2. J. W. Lee and J. M. Hyun, Double-diffusive convection in a rectangle with opposing horizontal temperature and concentration gradients, *Int. J. Heat Mass Transfer* **33,** 1619–1632 (1990).
3. J. W. Lee, M. T. Hyun and K. W. Kim, Natural convection in confined fluids with combined horizontal temperature and concentration gradients, *Int. J. Heat Mass Transfer* **31,** 1969–1977 (1988).
4. J. Patterson and J. Imberger, Unsteady natural convection in a rectangular cavity, *J. Fluid Mech.* **100,** 65–86 (1980).
5. G. N. Ivey, Experiments on transient natural convection in a cavity, *J. Fluid Mech.* **144,** 389–401 (1984).
6. S. G. Schladow, J. C. Patterson and R. L. Street, Transient flow in a side-heated cavity at high Rayleigh number: a numerical study, *J. Fluid Mech.* **200,** 121–148 (1989).
7. S. G. Schladow, Oscillatory motion in a side-heated cavity, *J. Fluid Mech.* **213,** 589–610 (1990).
8. S. Paolucci and D. R. Chenoweth, Transition to chaos in a differentially heated vertical cavity, *J. Fluid Mech.* **201,** 379–410 (1989).
9. R. Temam, On an approximate solution of the Navier–Stokes equations by the method fractional step: Part 1, *Arch. Ration. Mech. Analysis* **32,** 135–153 (1969).
10. J. Chang, T. F. Lin and C. H. Chien, Unsteady thermosolutal opposing convection of liquid–water mixture in a square cavity—I. Flow formation and heat and mass transfer characteristics, *Int. J. Heat Mass Transfer* **36,** 1315–1331 (1993).
11. R. K. Otnes and L. Enochson, *Applied Time Series Analysis.* Wiley, New York (1978).